Journal of Human Evolution 151 (2021) 102927

Contents lists available at ScienceDirect

Journal of Human Evolution

journal homepage: www.elsevier.com/locate/jhevol

Short Communications

Is ulna curvature in the StW 573 (‘Little Foot’) *Australopithecus* natural or pathological?

Isabella Araiza [a], Marc R. Meyer [b, *], Scott A. Williams [c, d]

[a] Department of Anthropology, University of California, Riverside, CA, 92521, USA
[b] Department of Anthropology, Chaffey College, Rancho Cucamonga, CA, 91737, USA
[c] Center for the Study of Human Origins, Department of Anthropology, New York University, 25 Waverly Place, New York, NY, 10003, USA
[d] New York Consortium in Evolutionary Primatology, New York, NY, 10024, USA

ARTICLE INFO

Article history:
Received 11 October 2020
Accepted 1 December 2020
Available online 25 December 2020

Keywords:
Hominin evolution
Functional anatomy
Australopithecus
Locomotion
Pathology

1. Introduction

The 3.67-million-year-old StW 573 (‘Little Foot’) *Australopithecus* from Sterkfontein, South Africa, is the most complete skeleton known in the hominin fossil record (Clarke and Tobias, 1995; Bruxelles et al., 2019; Clarke, 1998, 2019; Pickering et al., 2004). Characters for terrestrial bipedalism are accompanied by adaptations for climbing (Beaudet et al., 2019, 2020; Crompton et al., 2018; Heaton et al., 2019). The heavily damaged right ulna lacks any apparent curvature (Fig. 1), whereas the left ulna is better preserved and presents a high degree of curvature (Heaton et al., 2019). Despite severe postdepositional deformation of the ulnar shaft (Crompton et al., 2018), based on the observed asymmetry it has been averred that the straighter right ulna represents normal forearm morphology in ‘Little Foot’, while the extreme curvature of the left ulna is atypical, reflecting traumatic bowing of the left forearm resulting from a childhood fall (Crompton et al., 2018; Heile et al., 2018).

Acute plastic bowing deformities are common in the radius or ulna of children between the ages of four and ten years after a traumatic fall onto an outstretched hand, as juvenile bones are not fully ossified, with thinner cortex in absolute and relative terms, and have a high degree of elasticity relative to adults (Crowe and Swischuk, 1977; Stenstrom et al., 1978). If the force is greater than the strength of the bone, it undergoes plastic deformation, and when the force is released, the bone remains in its bowed position (Yamamoto, 2012). Plastic deformation is produced by numerous microfractures on the concave surface of the bone while preserving intact cortex on the convex surface (Kim et al., 2014). A fall on a hyperextended, pronated hand delivers maximal force along the radius, but with a few degrees of external rotation at the shoulder a maximal deforming force is delivered to the ulna (Aponte and Ghiatas, 1989; Kim et al., 2012). Most commonly, this presents clinically as bowing of ulna in lateral or medial view (Duckman et al., 1977). This type of injury can impinge normal supination and protonation if left untreated but often requires no intervention and heals with remodeling (Anderson et al., 1994).

By contrast, curvature is a normal anatomic feature of the ulna among extant apes and many early hominins (Howell and Wood, 1974; Drapeau et al., 2005). Diaphyseal curvature of the ulna and other long bones in mammals has traditionally been explained as an epigenetic reaction to locomotor behaviors where the limb is habitually loaded (Lanyon, 1980; Bertram and Biewener, 1988; Swartz, 1990; Milne, 2016; Henderson et al., 2017) and curvature results as bone is added to the compressed side of a bone shaft and resorbed from surfaces under tension (Frost, 1964, 1973). Recently, Milne (2016) explained ulnar diaphyseal curvature in terrestrial quadrupeds as an adaptation to the antigravity action of the triceps muscle resisting ground reaction forces. Forearm curvature in primates has been suggested to enhance the rotational efficiency of the pronator teres muscle (Trinkaus and Churchill, 1988; Aiello and Dean, 1990; Rose, 1993; Galtes et al., 2008). Henderson et al. (2017) explained shaft curvature in arboreal taxa as the habitual action of the brachialis muscle in maintaining elbow flexion. These explanatory mechanisms for ulna curvature are not mutually exclusive, as each reflects the participation of the forelimb in locomotor or postural behaviors. While radiographic evidence would definitively test the hypothesis of Heile et al. (2018), here we test whether the macroscopic diaphyseal curvature of the left ulna is similar to

---

* Corresponding author.
E-mail address: marc.meyer@chaffey.edu (M.R. Meyer).

https://doi.org/10.1016/j.jhevol.2020.102927

documented clinical cases of acute plastic bowing, or simply reflects a degree of curvature typical for apes and observed among many early hominins.

2. Materials and methods

Data for the StW 573 ulna were generated from 3D scans of the fossil taken by one of the authors (S.A.W.) at the University of the Witwatersrand in Johannesburg, South Africa (Fig. 2). The scan will be made freely available on MorphoSource in early 2021. The *Homo sapiens* sample ($n = 22$) is from fully fused adults from the Indian subcontinent from the Chaffey College human skeletal collection (10 male, 12 female). The human clinical data were collected from radiographs of eight recently diagnosed subadults who suffered acute plastic bowing of the forearm from published images in Borden (1975; $n = 4$), Yamamoto (2012; $n = 1$), and open source x-rays from Radiopaedia (2020; $n = 3$). It should be noted that despite a very small degree of partial correction by cortical remodeling, bowing would persist into adulthood without medical intervention (i.e., the arm is immobilized for several weeks in a plaster cast; Aponte and Ghiatas, 1989). Without medical intervention the individual suffers from appreciable limitations in supination and protonation (Crowe and Swischuk, 1977). Accordingly, humans uniformly perform medical interventions to correct the bowing, and as a result there are no available radiographic images of adults with plastic deformation of the ulna, necessitating the use of juvenile individuals for our comparative clinical sample. We caution that the use of radiographs in comparison to other image formats may introduce unwanted variation, as orientations may not be as standardized. Moreover, we acknowledge that ontogenetic effects are embedded in the clinical sample given that these are subadults.

Data for the following fossils were taken from published images: *Sahelanthropus tchadensis* ($n = 1$) represented by TM 266-01-050 (Guy et al., 2020); *Australopithecus afarensis* ($n = 2$) represented by A.L. 288 (Johanson et al., 1982) and A.L. 438−1 (Drapeau et al., 2005); *Paranthropus boisei* ($n = 2$) represented by OH 36 (Aiello et al., 1999) and L40-19 (Howell and Wood, 1974); *Australopithecus sediba* ($n = 1$) represented by U.W. 88−62 (Berger et al., 2010; Churchill et al., 2018); *Homo naledi* represented by U.W. 101−499 (Berger et al., 2015; Feuerriegel et al., 2017); and *Homo erectus* ($n = 2$) represented by KNM-WT 15000 (Brown et al., 1985; Walker and Leakey, 1993) and KNM-BK 66 (Solan and Day, 1992). Data for incomplete fossils A.L. 288−1 and OH 36 were collected from reconstructions in Drapeau et al. (2005), and fossil specimens OH 36 and L40-19 were mirrored for comparison to the left ulna of StW 573. Any variation in orientation of fossils would have confounding effects on shape analyses. Thus, we caution that analyses of the fossil ulnae taken from images in the literature rely on the accuracy of how the fossil was oriented, and here we assume that each was depicted in its correct anatomic orientation. The extant ape sample consists fully fused adult ulnae from *Pan troglodytes* ($n = 14$), *Gorilla beringei* ($n = 10$), *Pongo abelii* ($n = 13$), *Hylobates lar* ($n = 6$), and *Symphalangus syndactylus* ($n = 3$) from the Chaffey College skeletal collection and from 3D scans downloaded from MorphoSource (Supplementary Online Material [SOM] Table S1).

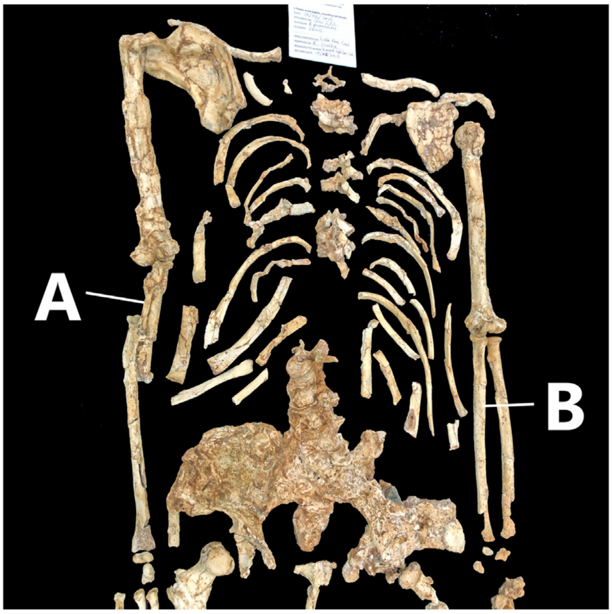

Figure 1. The upper skeleton of StW 573 illustrating differential preservation and condition of the right (A) and left (B) ulnae.

Data were collected from 2D images of the ulna in medial view and standardized to a 24-bit, 660 pixel width bitmap file. To isolate and standardize the diaphysis, fossil scans were cropped proximally just distal to the radial notch and distally at the point of minimum diaphysis width. The shaft of the ulna was similarly cropped at these landmarks in Henderson (2017: Fig. 1). Shape was assessed using the SHAPE package of programs (Iwata and Ukai, 2002) to generate elliptical Fourier descriptors (EFDs) of ulnar shaft contours to provide a mathematical accounting of shape variation. Principal component analysis was performed from coefficients of the EFDs to effectively summarize variation contained in the coefficients (Rohlf and Archie, 1984; Carlo et al., 2011).

Elliptical Fourier analysis has been shown to provide an accurate mathematical characterization of shape (Kaesler and Waters, 1972; Kuhl and Giardina, 1982; Persoon and Fu, 1977) and is a powerful biometric tool particularly suited for the description of fossils as it can delineate any type of shape with a closed two-dimensional contour (Athreya, 2009; Caple et al., 2017; Crampton, 1995; Schmittbuhl et al., 2007). As a result, elliptical shape analysis quantifies the entirety of the ulna shaft rather than a series of selected landmarks utilized in standard 2D geometric morphometrics. This method contrasts with Heile et al.'s (2018) measurement of ulnar diaphyseal curvature as the maximum distance from the posterior-most margin of the bone and a line drawn between two inflection points on the posterior margin of the diaphysis, one at the level of the radial notch and the other at the level of minimal distal circumference (curvature subtense; SOM Fig. S1). Long bone curvature subtense has several drawbacks relative to landmark

Figure 2. A) Render of a 3D model of the StW 573 left ulna, mirrored for demonstration purposes. B) Same as A with reconstructed area (gray) of the distal diaphysis by way of landmark matching with complete bone. C) Longitudinal section of the diaphysis isolated in this study for analysis per method of Henderson et al. (2017). See Materials and methods for further details on methodology.

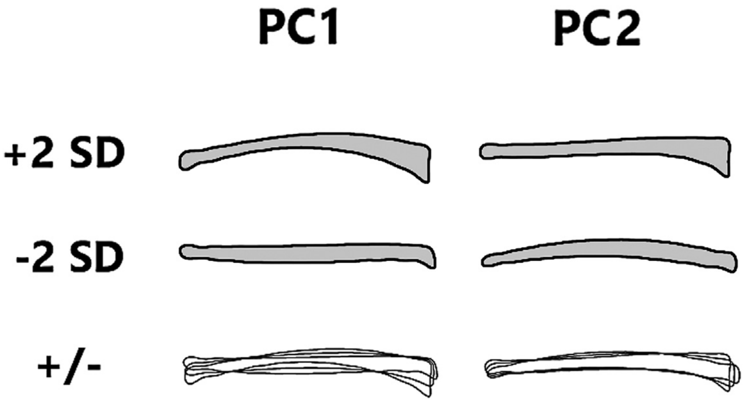

Figure 3. Shape variation within the first two principal components (PCs) produced from elliptical Fourier descriptors of ulnar shaft contours in medial view. PC1 (65.6% of variation) reflects midpoint curvature of the long axis of the ulna's diaphysis, with positive values representing a higher degree of curvature of both the posterior and anterior margins, and negative values representing straighter posterior and anterior margins. PC2 (15.3% of variation) reflects curvature of the posterior ulna shaft margin and the thickness of the ulna shaft toward its proximal aspect, with positive values representing a straight posterior margin and anteriorly thick proximal ulna diaphysis, and negative values representing a slightly curved posterior margin with a thinner proximal ulna shaft.

data collection, including a higher degree of measurement error (De Groote et al., 2010). To improve upon and avoid the drawbacks of using curvature subtense, we employ elliptical Fourier shape analysis which allows for shape quantification of the entire diaphysis.

3. Results

PC1 (65.6%) reflects midpoint curvature of the long axis of the ulna's diaphysis, with positive values representing a higher degree of curvature of both the posterior and anterior margins, and negative values representing straighter posterior and anterior margins (Fig. 3; SOM Fig. S1). PC1 largely distinguishes the human sample from the African great apes (with the latter exhibiting midpoint curvature). PC1 also partitions the more suspensory Asian apes from their more terrestrial African great ape counterparts, with the knuckle-walking African apes exhibiting more curved ulnae overall with greater robusticity toward the proximal aspect of the diaphysis.

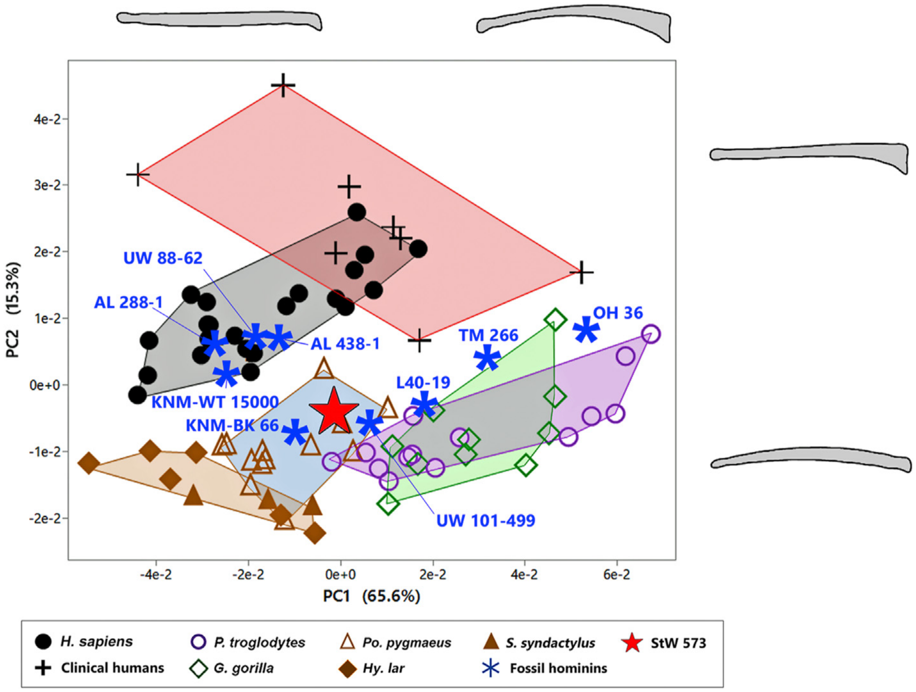

Figure 4. Biplot of the first two principal components (PCs) from elliptical Fourier descriptors of ulnar shaft contours in medial view. PC1 (65.6% of variation) reflects midpoint curvature of the long axis of the ulna's diaphysis, with positive values representing a higher degree of curvature of both the posterior and anterior margins, and negative values representing straighter posterior and anterior margins. PC2 (15.3% of variation) reflects curvature of the posterior ulna shaft margin and the margin and anteriorly thick proximal ulna diaphysis, and negative values representing a slightly curved posterior margin with a thinner proximal ulna shaft. The *Homo sapiens* distribution within the gray convex hull overlaps with the human clinical sample contained within the red convex hull. The convex hull of *Pongo* is shaded blue, *Pan* in purple, *Gorilla* in green, and hylobatids in orange. The following fossil specimens are included: TM 266 (*Sahelanthropus tchadensis*); A.L. 288−1 and A.L. 438−1 (*Australopithecus afarensis*); OH 36 and L40-19 (*Paranthropus boisei*); U.W. 88−62 (*Australopitheus sediba*); U.W. 101−499 (*Homo naledi*); KNM-WT 15000 and KNM-BK 66 (*Homo erectus*). (For interpretation of the references to color in this figure legend, the reader is referred to the Web version of this article.)

PC2 (15.3%) reflects curvature of the posterior ulna shaft margin and the thickness of the ulna shaft toward its proximal aspect, with positive values representing a straight posterior margin and thick proximal ulna diaphysis, and negative values representing a slightly curved posterior margin with a thinner proximal ulna shaft. The second principal component distinguishes humans and the human clinical sample from extant apes.

In a biplot of PC1 and PC2, none of the hominins, including the StW 573, falls within the human clinical sample morphospace (Fig. 4). The 'Little Foot' ulna falls squarely within the morphospace of *Pongo* along with the U.W. 101–499 *H. naledi* fossil from the Dinaledi chamber of the Rising Star cave system in the Cradle of Humankind, South Africa and the KNM-BK 66 *H. erectus* specimen from the Kapthurin Formation, Baringo, Kenya. With *Pongo* these three hominins exhibit a high degree of midshaft curvature and gracility discrete from modern humans.

As reported in the literature, the pathological clinical human sample tends to exhibit acute plastic bowing with curvature generally restricted to the convex posterior margin of the ulna shaft, with retention of a anteriorly thick proximal shaft (SOM Fig. S3). By contrast, the StW 573 ulna features a posteriorly curved ulna margin and a relatively thin, gracile proximal shaft inconsistent with clinical observations that place it outside the shape space expected for a case of acute plastic bowing. The gracile and slender overall appearance and thin proximal diaphysis of the StW 573 ulna differs with the more curved and robust TM-266-01-050 *Sa. tchadensis* and OH 36 and L40-19 *Pa. boisei* specimens, which fall closest to the shape space of *Pan* and *G. gorilla.* Each of the other hominin fossils (KNM-WT 15000, A.L. 288, A.L. 438, U.W. 88–62) falls within the human morphospace of humans and away from the human clinical sample.

4. Discussion and conclusions

As per gross morphological observations (Kim et al., 2014), elliptical Fourier analysis demonstrates in the human clinical sample that traumatic plastic deformation disturbs the concave posterior surface of the diaphysis, while preserving intact cortex morphology of the anterior convex surface. Although the use of radiographs in comparison to other image formats may have introduced unwanted variation, and ontogenetic effects are embedded in the clinical sample given that these are subadults, this is a detail that calculation of ulna shape by way of curvature subtense methodology fails to capture. As the StW 573 ulna falls outside the morphospace of the human clinical sample, our results fail to support the hypothesis that significant curvature of the StW 573 ulna is the result of traumatic bowing resulting from a childhood fall (Crompton et al., 2018; Heile et al., 2018). Instead, its position within the shape space of *Pongo* along with other hominins such as *H. naledi* and *H. erectus* from Baringo suggests that the high degree of curvature in the left forearm of the StW 573 *Australopithecus* represents normal anatomic variation. Moreover, these results suggest that the straightness of the heavily crushed right ulna is an artifact of postdepositional deformation that should not be taken as indicative of normal morphology. Other hominin ulnae display greater degrees of curvature with greater robusticity than StW 573, including *Paranthropus* and the newly announced *Sahelanthropus* fossil ulna, which appear most similar to the African great apes. Other fossil ulnae such as Nariokotome *H. erectus*, *A. afarensis* and *A. sediba* display a lesser degree of diaphyseal curvature, suggesting that the StW 573 forelimb had not been fully emancipated from a role in locomotion. This research adds to other observed postcranial adaptations for habitual loading of the forelimb (i.e., arboreality) in the remarkably complete 'Little Foot' skeleton.

Declaration of competing interest

The authors declare no conflict of interest.

Acknowledgments

The authors would like to thank the University of the Witwatersrand curator of collections Bernhard Zipfel and collections manager Sifelani Jirah for facilitating access to the StW 573 fossil. We are grateful to the L.S.B. Leakey Foundation for financially supporting this research. We would like to thank our editor David Alba, the associate editor, and Jason Heaton and two anonymous reviewers for their constructive comments on a previous draft which greatly improved this manuscript.

Supplementary Online Material

Supplementary Online Material to this article can be found online at https://doi.org/10.1016/j.jhevol.2020.102927.

References

Aiello, L., Dean, C., 1990. An Introduction to Human Evolutionary Anatomy. Academic Press, London.

Aiello, L.C., Wood, B., Key, C., Lewis, M., 1999. Morphological and taxonomic affinities of the Olduvai ulna (OH 36). Am. J. Phys. Anthropol. 109, 89–110.

Anderson, I.F., Hume, K.F., Chong, A.L., 1994. Plastic bowing of the forearm in the more mature skeleton. Aust. N. Z. J. Surg. 64, 132–134.

Aponte, J.E., Ghiatas, A., 1989. Acute plastic bowing deformity: A review of the literature. J. Emerg. Med. 7, 181–184.

Athreya, S., 2009. A comparative study of frontal bone morphology among Pleistocene hominin fossil groups. J. Hum. Evol. 57, 786–804.

Beaudet, A., Clarke, R.J., Bruxelles, L., Carlson, K.J., Crompton, R., de Beer, F., Dhaene, J., Heaton, J.L., Jakata, K., Jashashvili, T., Kuman, K., McClymont, J., Pickering, T.R., Stratford, D., 2019. The bony labyrinth of StW 573 ("Little Foot"): Implications for early hominin evolution and paleobiology. J. Hum. Evol. 127, 67–80.

Beaudet, A., Clarke, R.J., Heaton, J.L., Pickering, T.R., Carlson, K.J., Crompton, R.H., Jashashvili, T., Bruxelles, L., Jakata, K., Bam, L., Van Hoorebeke, L., Kuman, K., Stratford, D., 2020. The atlas of StW 573 and the late emergence of human-like head mobility and brain metabolism. Sci. Rep. 10, 4285.

Berger, L.R., de Ruiter, D.J., Churchill, S.E., Schmid, P., Carlson, K.J., Dirks, P.H., Kibii, J.M., 2010. *Australopithecus sediba*: a new species of *Homo*-like australopith from South Africa. Science 328, 195–204.

Berger, L.R., Hawks, J., de Ruiter, D.J., Churchill, S.E., Schmid, P., Delezene, L.K., Kivell, T.L., Garvin, H.M., Williams, S.A., DeSilva, J.M., Skinner, M.M., Musiba, C.M., Cameron, N., Holliday, T.W., Harcourt-Smith, W., Ackermann, R.R., Bastir, M., Bogin, B., Bolter, D., Brophy, J., Cofran, Z.D., Congdon, K.A., Deane, A.S., Dembo, M., Drapeau, M., Elliott, M.C., Feuerriegel, E.M., Garcia-Martinez, D., Green, D.J., Gurtov, A., Irish, J.D., Kruger, A., Laird, M.F., Marchi, D., Meyer, M.R., Nalla, S., Negash, E.W., Orr, C.M., Radovcic, D., Schroeder, L., Scott, J.E., Throckmorton, Z., Tocheri, M.W., VanSickle, C., Walker, C.S., Wei, P., Zipfel, B., 2015. *Homo naledi*, a new species of the genus *Homo* from the Dinaledi Chamber, South Africa. eLife 4, e09560.

Bertram, J.E.A., Biewener, A.A., 1988. Bone curvature: sacrificing strength for load predictability? J. Theor. Biol. 131, 75–92.

Borden, S., 1975. Roentgen recognition of acute plastic bowing of the forearm in children. Am. J. Roentgenol. 125, 524–530.

Brown, F., Harris, J., Leakey, R., Walker, A., 1985. Early *Homo erectus* skeleton from west Lake Turkana, Kenya. Nature 316, 788–792.

Bruxelles, L., Stratford, D.J., Maire, R., Pickering, T.R., Heaton, J.L., Beaudet, A., Kuman, K., Crompton, R., Carlson, K.J., Jashashvili, T., McClymont, J., Leader, G.M., Clarke, R.J., 2019. A multiscale stratigraphic investigation of the context of StW 573 'Little Foot' and Member 2, Sterkfontein Caves, South Africa. J. Hum. Evol. 133, 78–98.

Caple, J., Byrd, J., Stephan, C.N., 2017. Elliptical Fourier analysis: fundamentals, applications, and value for forensic anthropology. Int. J. Leg. Med. 131, 1675–1690.

Carlo, J.M., Barbeitos, M.S., Lasker, H.R., 2011. Quantifying complex shapes: elliptical Fourier analysis of octocoral sclerites. Biol. Bull. 220, 224–237.

Churchill, S., Green, D., Feuerriegel, E., Macias, M., mathews, s., Carlson, K., Schmid, P., Berger, L., 2018. Special Issue: *Australopithecus sediba*: The shoulder, arm, and forearm of *Australopithecus sediba*. PaleoAnthropology 2018, 234–281.

Clarke, R.J., 1998. First ever discovery of a well-preserved skull and associated skeleton of *Australopithecus*. S. Afr. J. Sci. 94, 460–464.

Clarke, R.J., 2019. Excavation, reconstruction and taphonomy of the StW 573 *Australopithecus prometheus* skeleton from Sterkfontein Caves, South Africa. J. Hum. Evol. 127, 41–53.

Clarke, R.J., Tobias, P.V., 1995. Sterkfontein Member 2 foot bones of the oldest South African hominid. Science 269, 521–524.

Crampton, J.S., 1995. Elliptic Fourier shape analysis of fossil bivalves: some practical considerations. Lethaia 28, 179–186.

Crompton, R.H., McClymont, J., Thorpe, S., Sellers, W., Heaton, J., Pickering, T.R., Pataky, T., Stratford, D., Carlson, K., Jashashvili, T., Beaudet, A., Bruxelles, L., Goh, C., Kuman, K., Clarke, R., 2018. Functional anatomy, biomechanical performance capabilities and potential niche of StW 573: an *Australopithecus* skeleton (circa 3.67 Ma) from Sterkfontein Member 2, and its significance for the last common ancestor of the African apes and for hominin origins. bioRxiv. https://doi.org/10.1101/481556.

Crowe, J.E., Swischuk, L.E., 1977. Acute bowing fractures of the forearm in children: a frequently missed injury. Am. J. Roentgenol. 128, 981–984.

De Groote, I., Lockwood, C., Aiello, L., 2010. Technical note: a new method for measuring long bone curvature using 3D landmarks and semi-landmmarks. Am. J. Phys. Anthropol. 141, 658–664.

Drapeau, M.S., Ward, C.V., Kimbel, W.H., Johanson, D.C., Rak, Y., 2005. Associated cranial and forelimb remains attributed to *Australopithecus afarensis* from Hadar, Ethiopia. J. Hum. Evol. 48, 593–642.

Duckman, H.H., Ambrose, J.F., Iulo, A.D., 1977. Traumatic bowing of the forearm bones in children. J. Am. Coll. Emerg. Phys. 6, 100–102.

Feuerriegel, E.M., Green, D.J., Walker, C.S., Schmid, P., Hawks, J., Berger, L.R., Churchill, S.E., 2017. The upper limb of *Homo naledi*. J. Hum. Evol. 104, 155–173.

Frost, H.M., 1964. The Laws of Bone Structure. Thomas, Springfield.

Frost, H.M., 1973. Bone Modeling and Skeletal Remodeling Errors. Charles C Thomas, Springfield.

Galtes, I., Jordana, X., Cos, M., Malgosa, A., Manyosa, J., 2008. Biomechanical model of pronation efficiency: new insight into skeletal adaptation of the hominoid upper limb. Am. J. Phys. Anthropol. 135, 293–300.

Guy, F., Daver, G., Taisso Mackaye, H., Likius, A., Boisserie, J.-R., Moussa, A., Vignaud, P., Nekoulnang, C., 2020. Postcranial evidence of late Miocene hominin bipedalism in Chad. Nature Research. https://doi.org/10.21203/rs.3.rs-69453/v1.

Heaton, J.L., Pickering, T.R., Carlson, K.J., Crompton, R.H., Jashashvili, T., Beaudet, A., Bruxelles, L., Kuman, K., Heile, A.J., Stratford, D., Clarke, R.J., 2019. The long limb bones of the StW 573 *Australopithecus skeleton* from Sterkfontein Member 2: Descriptions and proportions. J. Hum. Evol. 133, 167–197.

Heile, A.J., Pickering, T.R., Heaton, J.L., Clarke, R.J., 2018. Bilateral asymmetry of the forearm bones as possible evidence of antemortem trauma in the StW 573 Australopithecus skeleton from Sterkfontein Member 2 (South Africa). bioRxiv. https://doi.org/10.1101/486076.

Henderson, K., Pantinople, J., McCabe, K., Richards, H.L., Milne, N., 2017. Forelimb bone curvature in terrestrial and arboreal mammals. PeerJ 5, e3229.

Howell, F.C., Wood, B.A., 1974. Early hominid ulna from the Omo basin, Ethiopia. Nature 249, 174–176.

Iwata, H., Ukai, Y., 2002. SHAPE: A computer program package for quantitative evaluation of biological shapes based on elliptic fourier descriptors. J. Hered. 93, 384–385.

Johanson, D.C., Lovejoy, C.O., Kimbel, B., White, T.D., Ward, S.C., Bush, M.E., Latimer, B.M., Coppens, Y., 1982. Morphology of the Pliocene partial Hominid skeleton (A.L. 288-1) from the Hadar Formation, Ethiopia. Am. J Phys. Anthrol 57, 432–451.

Kaesler, R.L., Waters, J.A., 1972. Fourier analysis of the ostracod margin. Bull. Geol. Soc. Am. 83, 1169–1178.

Kim, E., Moritomo, H., Murase, T., Masatomi, T., Miyake, J., Sugamoto, K., 2012. Three-dimensional analysis of acute plastic bowing deformity of ulna in radial head dislocation or radial shaft fracture using a computerized simulation system. J. Shoulder Elbow Surg. 21, 1644–1650.

Kim, Y.S., Lee, H.M., Kim, J.P., Lim, C.R., 2014. Unusual presentation of a type 1 Monteggia equivalent lesion: simultaneous medial humeral condyle fracture with ipsilateral anterior dislocation of the radial head and acute plastic bowing of the ulna. J. Pediatr. Orthop. B 23, 383–388.

Kuhl, F.P., Giardina, C.R., 1982. Elliptic Fourier features of a closed contour. Comput. Graph. Image Process. 18, 236–258.

Lanyon, L.E., 1980. The influence of function on the development of bone curvature. An experimental study on the rat tibia. J. Zool. 192, 457–466.

Milne, N., 2016. Curved bones: An adaptation to habitual loading. J. Theor. Biol. 407, 18–24.

Persoon, E., Fu, K., 1977. Shape discrimination using Fourier descriptors. IEEE Transactions on Systems, Man, and Cybernetics 7, 170–179.

Pickering, T.R., Clarke, R.J., Heaton, J.L., 2004. The context of Stw 573, an early hominid skull and skeleton from Sterkfontein Member 2: taphonomy and paleoenvironment. J. Hum. Evol. 46, 277–295.

Radiopaedia.org, 2000. Bowing fracture: rID: 25294. https://radiopaedia.org/articles/bowing-fracture. (Accessed September 2020).

Rohlf, F.J., Archie, J.W., 1984. A comparison of Fourier methods for the description of wing shape in mosquitoes (Diptera: Culicidae). Syst. Biol. 33, 302–317.

Rose, M.D., 1993. Functional anatomy of the elbow and forearm in primates. In: Gebo, D.L. (Ed.), Postcranial Adaptation in Nonhuman Primates. Northern Illinois University Press, DeKalb, pp. 70–95.

Schmittbuhl, M., Rieger, J., Le Minor, J.M., Schaaf, A., Guy, F., 2007. Variations of the mandibular shape in extant hominoids: Generic, specific, and subspecific quantification using elliptical fourier analysis in lateral view. Am. J. Phys. Anthropol. 132, 119–131.

Solan, M., Day, M.H., 1992. The Baringo (Kapthurin) ulna. J. Hum. Evol. 22, 307–313.

Stenstrom, R., Gripenberg, L., Bergius, A.R., 1978. Traumatic bowing of forearm and lower leg in children. Acta Radiol. Diagn. 19, 243–249.

Swartz, S.M., 1990. Curvature of the forelimb bones of anthropoid primates: Overall allometric patterns and specializations in suspensory species. Am. J. Phys. Anthropol. 83, 477–498.

Trinkaus, E., Churchill, S.E., 1988. Neandertal radial tuberosity orientation. Am. J. Phys. Anthropol. 75, 15–21.

Walker, A., Leakey, R.E. (Eds.), 1993. The Nariokotome*Homo erectus* Skeleton. Harvard University Press, Cambridge.

Yamamoto, L.G., 2012. Reduction of bowing forearm fractures in the ED under propofol sedation. Am. J. Emerg. Med. 30, 249.e1–249.e4.